Pressure Waves in a Far-field Repetitive Pulse Laser Thruster*

Koichi MORI, Hiroshi KATSURAYAMA, Kimiya KOMURASAKI, and Yoshihiro ARAKAWA
University of Tokyo, Hongo 7-3-1, Bunkyo, Tokyo 113-8656, Japan
e-mail: mori@al.t.u-tokyo.ac.jp

IEPC-01-205

Plasma expansion and resulting pressure wave propagation were investigated by experiments. A 10-J-CO_2 pulse laser beam was focused in the quiescent atmospheric air, and plasma was generated. The density discontinuity around plasma was visualized using the shadowgraphs and the pressure imparted on a flat plate was measured using a pressure gauge. It was found that the Mach number and the blast wave pressure in the far-field can be predicted by the Mach number at the characteristic point in the near-field. By applying an explosion source model to CFD simulations, the impulse of RP laser thruster will be predicted easily.

Introduction

Laser propulsion will serve as an alternative rocket system both for ground-to-orbit launch and for orbit transfer in near future. Myrabo *et al.* are conducting laser propulsion flight tests with a scale model "Light Craft." [1] Their scale model utilizes an atmospheric air as a propellant. Because it is not necessary to load a propellant on board for the atmospheric flight, the payload ratio is improved remarkably. This type of thruster can be categorized as "Air-breathing RP (Repetitive Pulse) laser thruster." The orbital launch of one-kilogram payloads will require a megawatt laser. A conceptual far-field laser thruster is illustrated in Fig.1. In the RP laser propulsion, the thrust is imparted by the explosive expansion of laser-produced plasma. When a laser beam is focused in the atmospheric air, breakdown occurs near the focus. The laser-produced plasma absorbs the following part of the laser pulse.

Many researches have been conducted on formation and expansion of laser plasma in a quiescent atmospheric air. [2-5] The infrared laser is absorbed through the inverse-bremstrahlung (IB) emission, whose absorption coefficient is proportional to the square of electron density. Plasma propagates along the laser light channel and expands outward during the laser irradiance. Among many theoretical models, a propagation model proposed by Raizer [6] is often referred to. In the model, at the laser fluxes greater than 10^7 W/cm^2, plasma heating is in the Laser Supported Detonation (LSD) regime. At the fluxes of $10^6 \sim 10^7$ W/cm^2, it is in Laser Supported Combustion (LSC) regime.

In the LSD regime, the incident laser energy is absorbed in the plasma attached with a shock wave. Because the plasma is compressed and heated by the leading shock wave and the electron density is increased, the absorption is thought to occur more efficiently than without the shock wave. The absorbed energy is converted into the kinetic energy of the expanding gas, which drives the LSD wave and supports the leading shock wave.

In the LSC regime, the shock wave has decayed and does not interact with the laser beam. Heating processes are dominated by diffusive mechanisms: The atmosphere surrounding the plasma is heated and ionized through the thermal conduction from plasma, and a pre-ionized region is generated. At the side of the laser incidence, the laser beam heats the pre-heated region. The heated region expands in the direction opposite to the laser beam at a sub-sonic speed.

In either regime, the laser absorption and plasma expansion depend on the laser energy, history of the laser pulse, and *F*-number of the optics (=focal length / beam diameter), etc.

Especially in the LSD regime, the plasma has pressure much higher than the atmospheric pressure in the near-field. The quick expansion of high-pressure plasma drives a blast wave outward in the far-field.

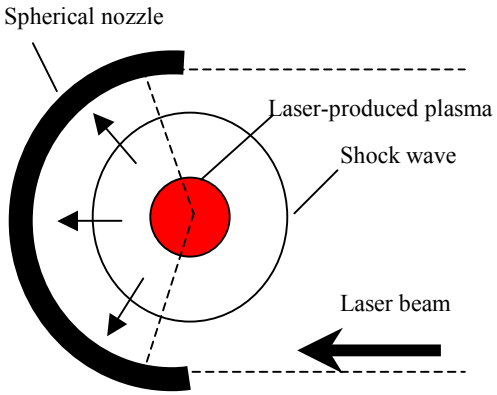

Fig.1 A conceptual far-field laser thruster

The blast wave is defined as a flow field induced by the leading shock wave. Because the shock wave is followed by the rarefaction waves, the typical spherical blast wave consists of a leading positive gauge pressure phase and a following negative gauge pressure phase.

If the energy input occurs instantaneously, and the explosion is strong, the propagation and the structure of the blast wave can be predicted by the Sedov solution. [7] In the solution, the blast wave structure and the impulse are determined only by the energy given in the explosion source. The strength of the shock wave is defined by the ratio of the over-pressure of the shock wave to the atmospheric pressure, and Sedov solution holds its validity in the case that the ratio is much higher than $(\gamma+1)/(\gamma-1)\cdot p_0$. Here, γ is the specific heat ratio, and p_0 is the atmospheric pressure.

In contrast, in the weak explosions, the source motion governs the blast wave structure, and various properties of the source would give various blast wave structures. Boundary conditions govern the reflection and diffraction of the blast wave and the affect the resultant impulse imparted on the boundary.

The nozzle should be optimized to maximize the impulse imparted on its inner-surface. Because the heating and expansion processes are not stationary, the design rules for conventional rocket nozzle cannot be applied to this thruster design. To establish the design rules, the impulsive thrust should be estimated in the arbitrary set of the conditions such as the laser power, *F*-number of the optics, and the nozzle shape. Although CFD simulations would be suited for the purpose, the heating and the expansion of the plasma, or in other word, the phenomena governing the explosion in the near-field, is still hard to predict because it must contain non-equilibrium thermochemical reactions. [8] Developing a simple model for the explosion source is very useful for CFD simulations. This study presents an explosion source condition for a given condition by deducing from the shadowgraphs and the pressure measurement. The explosion source condition would be a function of the laser power, its history and the *F*-number of the optics.

Experimental facilities

A 10-J-pulse TEA CO_2 laser was used for the experiments. The history of laser power, which is shown in Fig. 2, was measured using a photon-drag CO_2 laser detector (Hamamatsu photonics-B749). A leading-edge spike appears, which is followed by slowly decaying tail. The cross section of the laser beam is a square of 30 × 30 mm. Laser beam was focused using an off-axial parabola mirror, whose focal length is 19.1 mm and *F*-number is 1.1.

The laser-heating processes were observed by the shadowgraph method using an ICCD camera (Oriel Instruments InstaSpec^{TM}V ICCD detector, Model77193-5) with high-speed gating. The experimental setup is illustrated in Fig. 3. The image intensifier of the camera was operated as a shutter. An optical emission from a gap-switch of laser discharge tube was utilized to trigger the shutter: The strong emission from the gap-switch before the beginning of the laser irradiance is detected by a photo-sensor through an optical fiber. The photo-sensor signal is transmitted to a delay-circuit (Stanford Research

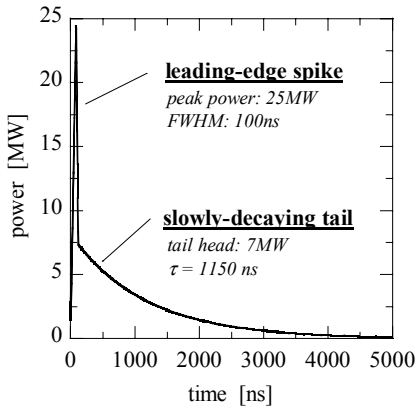

Fig.2 The history of the laser power

Systems, Inc. Digital Delay/Pulse Generator Model DG535), which enabled us to take a picture with any delay period from the beginning of the laser irradiance.

A He-Ne laser was used as a light source for shadowgraphs. A band-path filter transmitting the wavelength of 633 ± 10 nm was inserted between plasma and the camera. The observed image is the superpose of the shadowgraph and the bremstlahlung radiation from plasma. Since the strength of bremstlahlung radiation is proportional to the square of free electron density, the strongly emitting region in the images would be identical to a highly ionized region. Since the absorption is dominated by the inverse-bremstrahlung effect, the highly emitting region is thought to absorb the laser energy. The pictures were taken from $t = 0\ \mu$ s, when the laser pulse incidence begins, to $t = 6\ \mu$ s. Because the total duration of the laser pulse is $5\ \mu$ s, the pictures were taken almost during the laser irradiance. Exposure period was 250ns for each picture

Blast wave pressure was measured using a quartz pressure gauge (Kistler-603B) that responds to high-frequency pressure variation with its natural frequency 400kHz. The gauge head is placed on a flat plate, whose surface is a square of $20\text{mm} \times 20\text{mm}$. The natural frequency of charge-amplifier (Kistler 5011B10Y26) is 200kHz, which limits the response to the high frequency variation of pressure. Although the measured time-scale of blast wave is the order of the $100\ \mu$ s, this upper frequency limit of amplifier influences only on the response to the peak pressure,

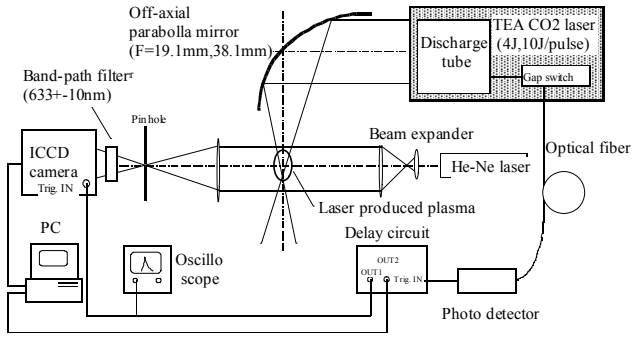

Fig.3 Experimental setup

100Hz. Because the total duration of the blast wave is less than 1ms, this lower limit has no influence on which is measured when the shock wave is reflected on the plate.. The gauge is placed at $r = 30$mm, and is lineally moved to 50mm along the axis by 5mm. r is the distance between the focus and the gauge head.

Results and discussions

Visualization of the near-field shock wave

Shadowgraphs were shown in Fig. 4. Laser beam is coming from the topside of each picture. At $t = 0\ \mu$ s, a strongly emitting point appears at the focus. The breakdown of air occurs. After the breakdown, the shock wave propagates outward and at the side of laser incidence, the shock wave attached by strongly emitting plasma propagates along the light channel opposite to the direction of the laser incidence. The plasma behind the shock wave is heated through the laser absorption, and that is in the LSD regime heating. At $t = 2.5\ \mu$ s, the shock wave leaves off the plasma, and the LSD regime ends. The shock wave propagates outward farther, and its velocity decays slowly. The propagation velocity of the plasma front decays instantaneously, and the strength of the emission from the plasma also decays.

The LSD wave propagates elliptically, and the center of explosion moves during the laser incidence. The center of elliptic discontinuity, and the ratio of its longer to shorter radii are plotted in Fig.5. The center moves along the laser axis opposite to the laser incidence and then stops. The resultant displacement from the focus is not so large as the radius. The ratio of the radii changes at the early stage of the laser incidence, and it reaches a constant value at the later stage. As a result, the ratio becomes almost unity and the expansion becomes approximately spherical. This would be because the F-number of the optics was comparably small. If the F-number were larger, the ratio of radii and the displacement of explosion center would have been larger than that in this case. Although these small differences of the center position and the radii would not have significant effects in the far-field, where the considering scale is much larger than that in the near-field, the differences would have significant effects on the laser heating processes.

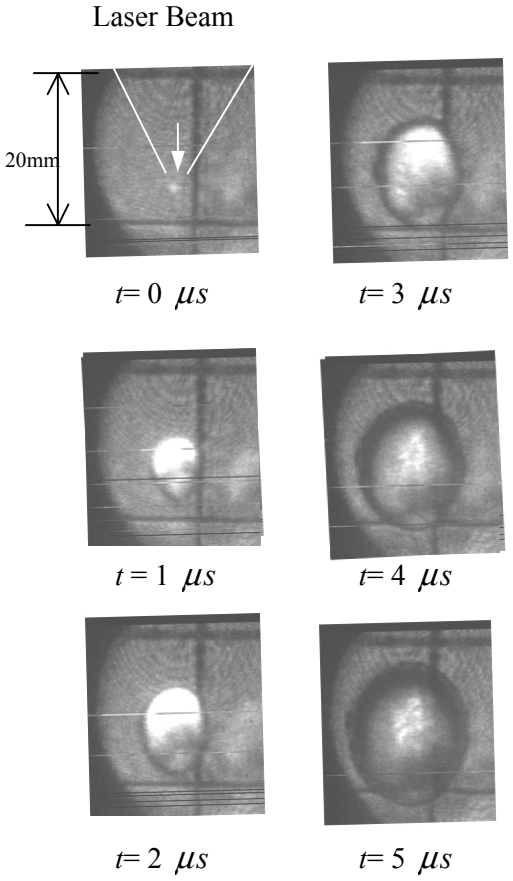

Fig.4 Shadowgraphs in the vicinity of the laser focus.

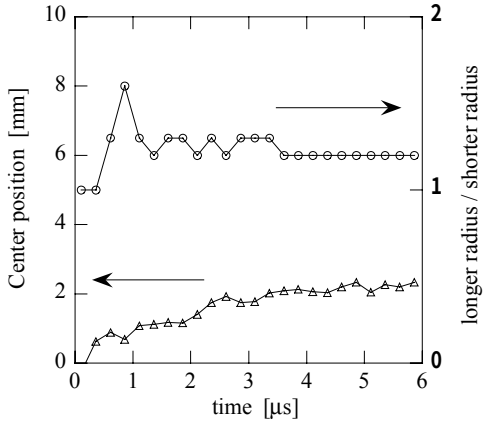

Fig.5 The time history of center poison of the elliptic plasma and the ratio of the longer radius to the shorter radius of the plasma.

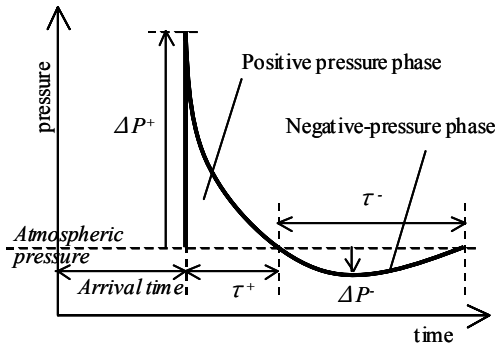

Figure 6 The typical time history and characteristic variables of blast wave.

Pressure wave measurement in the far-field

Typical structure of the blast wave at the far-field is illustrated in Fig.6. There are two independent properties: propagation velocity U and width of the positive pressure pulse τ^+ determining the impulse contributed from the positive pressure phase. The minimum increment of negative pressure phase Δp^- and the phase duration τ^- characterize the shape of the negative pressure phase. These characteristic values would be governed by the wave motion at the near-field.

Arrival time and Mach number of the shock wave

Whitham has formulated the three-dimensional propagation of the shock waves [9], and this technique predicting the shock wave propagation is called as the geometric shock dynamics. In the case of spherical shock waves, analytical formulation becomes very simple. The relation between the radius of spherical shock wave r and its propagation Mach number M is determined by the set of the initial values (r_0, M_0). The formula is gives as,

$$M = [\{(M_0^{\,2} - 1) r_0^{\,2K}\} r^{-2K} + 1]^{1/2} \qquad (1)$$

K is the weak function of the Mach number. In the limit of the strong shock wave ($M \to \infty$), K is 0.394, and in the weak limit ($M \to 1$), K is 0.5. The Mach number decays as the wave propagates.

Once the Mach number of shock wave at the characteristic radius of near-field: $r_0 = 0.15\ R^*$ is given as M_0, the Mach number in the far-field is determined. R^* is an effective radius of a blast wave, and defined as:

$$R^* = (E_0 / P_0)^{1/3} \qquad (2)$$

This is the radius where the over-pressure of blast wave reaches the order of atmospheric pressure.

In Fig.7, the relationship between the radius of the shock wave and its arrival time is plotted on the (r, t) plane. In the near-field, the data were taken from the shadowgraphs, and in the far-field, the data were obtained from the pressure gauge measurement. Mach number of the shock wave estimated using Fig.7 is plotted in Fig.8. After the laser irradiance, the Mach number decreases moderately as the wave propagates into the far-field, and approaches to unity.

Assigning the measured Mach number at $r_0 = 0.15\ R^*$ (or the *initial point* as noted in the figure) into the equation (1), the Mach number variation in the far-field was estimated. The Solid curve represents the theoretical values at the weak shock limit ($M \to 1$), and the broken curve, at the strong shock limit ($M \to \infty$). The differences between both curves are small. The theoretical values agree well but are somehow overestimating.

Peak pressure

Because the shock wave reflects normally to the flat plate, on which the pressure gauge head is fixed, the pressure behind the reflected shock wave was measured. In Fig.9, the peak pressure is plotted. The pressure decays with r. Rankine-Hugoniot law gives the relationship between the propagation Mach number of the shock wave and the pressure behind the wave. The triangles in Fig.9 are the pressure estimated from the Mach number. The values are the pressure behind the shock wave reflected normally on the plate. The estimated and the measured pressures are very close to each other, indicating that the peak pressure and the Mach number are measured consistently. The solid curve is the theoretical pressure calculated using the equation (1) in the weak shock limit. Because the theory overestimates the Mach number at the far field, the pressure is also overestimated.

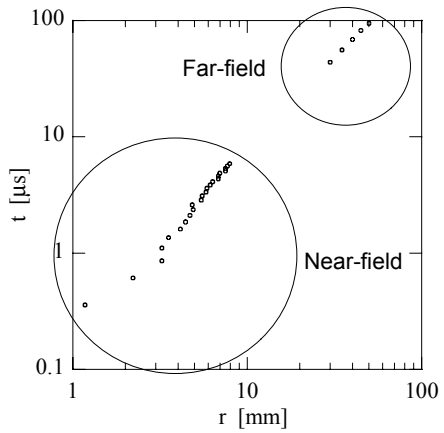

Fig.7 The *r-t* diagram in the near-field and far-field.

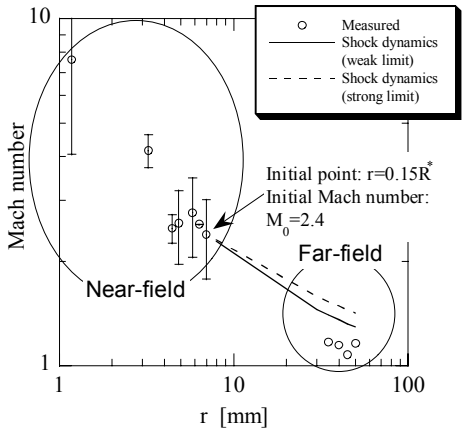

Fig.8 Mach number of the shock wave.

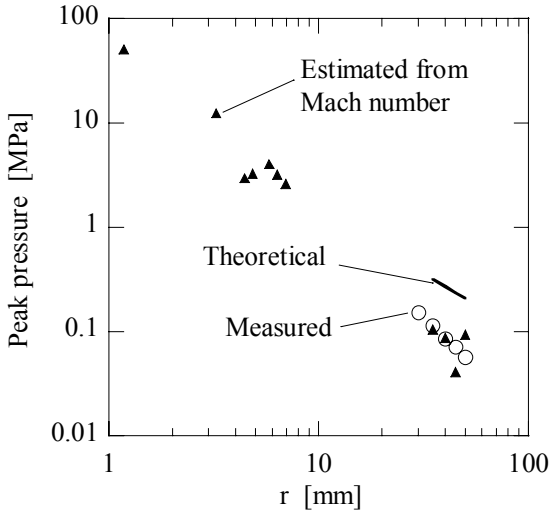

Fig.9 Peak pressure of the reflected blast wave.

Summary

The shock wave was found to propagate almost spherically in the near-field with a focusing optics of F=1.1. The propagation Mach number of the leading shock wave decays as the wave propagates. It was suggested that the Mach number would be predicted by the geometric shock dynamics. The initial Mach number M_0 (in experiment, it was 2.4) at the characteristic source radius $r_0 = 0.15R^*$ can be used as the explosion source in the CFD simulations.

M_0 would vary depending on the laser power, F-number of the optics, and ambient pressure etc. In the future work, the dependency of M_0 on these conditions will be investigated.

References

[1] Myrabo, L.M., "Ground and Flight Tests of a Laser propelled Vehicle," AIAA Paper 98-1001.

[2] Weyl, G., Pirri, A., Root, R., "Laser Ignition of Plasma Off Aluminum Surface," *AIAA Journal* Vol.19, No.4, pp.460-469, 1981.

[3] Reilly, J.P., Ballantyne, A., Woodroffe, J.A., "Modeling of Momentum Transfer to a Surface by Laser-Supported Absorption Waves," *AIAA Journal* Vol.17, No.10, pp.1098-1105, 1978.

[4] Barchukov, A.I., Bunkin, F.V., Konov, V.I., Lyubin, A.A., "Investigation of low-threshold gas breakdown near solid targets by CO_2 laser radiation," *Sov.Phys.-JETP*, Vol.39, No.3, pp.469-477, 1974.

[5] Raizer, Y.P., "Breakdown and Heating of Gases under the Influence of a Laser Beam," *Sov.Phys.USPEKHI*, Vol.8, No.5, pp.650-673, 1966.

[6] Raizer, Y.P.: *Laser-Induced Discharge Phenomena*, Studies in Soviet Science, Consultants Bureau, New York, 1977.

[7] Zel'dovich, Y.B., Raizer, Y.P., *Physics of Shock waves and High-Temperature Hydrodynamic Phenomena*, Academic Press, New York, 1966.

[8] Jonathan E.J. and Ten-See W., "Time dependent measurement of electron temperature and density in a Laser Lightcraft," AIAA paper 2001-3796.

[9] G.B.Whitham: *Linear and Nonlinear Waves*, John Wiley & Sons, New York,1999.